Master of Aerospace Engineering Research Project

HALE AEROECODESIGN

S2 Project report

Author: Víctor Manuel Guadaño Martín

Due date of report: 22/06/2020
Actual submission date: 21/06/2020

Starting date of project: 28/01/2020 Duration: 14 Months

Tutors: J. Morlier, E. Duriez

Declaration of Authenticity

This assignment is entirely my own work. Quotations from literature are properly indicated with appropriated references in the text. All literature used in this piece of work is indicated in the bibliography placed at the end. I confirm that no sources have been used other than those stated.

I understand that plagiarism (copy without mentioning the reference) is a serious examinations offence that may result in disciplinary action being taken.

Date: 21/06/2020

Signature:

Víctor Manuel GUADAÑO MARTÍN

Abstract

Multidisciplinary Design Optimization (MDO) allows to find an optimum for the interaction of disciplines, which leads to a better solution than by optimizing each discipline independently. The CO_2 footprint optimization of a solar-powered High Altitude Long Endurance (HALE) drone is studied.

This optimization is performed using a modified version of OpenAeroStruct, a tool for aerostructural optimization based on OpenMDAO, which is an optimization framework that allows analytic derivatives to be propagated through the models and passed to a gradient-based optimizer.

The main issue of this work is to improve the optimization in terms of both results and performance by making some changes in the modified version of OpenAeroStruct used. This version includes material choice optimization for the structure of the HALE in the MDO approach. This feature is improved by adding the analytic derivatives for gradient-based optimization. Moreover, engines are included in the model of the HALE allowing the optimization to vary their position for better results. The simple HALE model developed shows acceptable agreement with more complex models.

Keywords: Multidisciplinary design optimization, eco-conception, high-altitude long endurance drone, aerostructural design optimization, OpenAeroStruct

Table of Contents

1 Introduction

A low-fidelity multidisciplinary optimization tool for High Altitude Long Endurance (HALE) aircraft is being developed from OpenAeroStruct. A defining feature of high-aspect ratio HALE vehicles is the tight coupling between aerodynamics and structure. OpenAeroStruct allows to perform aerostructural optimization using OpenMDAO, a multidisciplinary design optimization framework.

In [1], material choice was successfully integrated in the tool in order to optimize the CO_2 emissions of the HALE. With this feature, the optimization is capable of choosing among a discrete catalogue of materials in the form of a continuous variable, required in MDO approach with continuous optimization algorithms.

In this work, analytic partial derivatives are added to the tool, allowing the material selection to use gradient-based optimization. This leads to more efficient and accurate optimizations. Besides, the engines has been added to the model, considering their spanwise position as a new design variable that the optimization can modify. The engines reduce the bending moment on the wing due to lift achieving more realistic results that can be perfectly compared to those of a more complex model with higher fidelity, such as the one presented in [2].

2 Semester 2 section

2.1 Context and key issues

All gradient based solvers converge to a locally optimal point. And gradient-based optimization algorithms scale much better with the number of design variables than gradient-free methods, which is very important for multidisciplinary design optimization. Nevertheless, gradient based solvers converge to a locally optimal point, so, the reach of a global optimum depends heavily on the starting point of the optimization.

Accordingly, one of the major problems to face is the convergence of the optimizations, since the model could be very close to reality but the starting points must be chosen carefully to reach an optimum. For this reason, it is important to achieve a compromise solution between the convergence of the optimization and the complexity of the model. Finding this equilibrium is the central issue of the project.

2.2 State of the art

High-Altitude Long Endurance (HALE) is the description of an air-borne vehicle which functions optimally at high-altitude (around 60000 ft) and is capable of flights which last for considerable periods of time without recourse to landing. They are also called *atmospheric satellites* or *atmosats* because their development is focused towards providing services conventionally provided by artificial satellites orbiting in space. One of the main advantages of HALE drones, apart from being powered by solar energy, is that they are environment-friendly and much cheaper than satellites.

As no fuel is burned during the operation of HALE drones, their CO_2 emissions come from the manufacturing and the materials. Therefore, continuing the work presented in [1], this is what will be optimized.

Multidisciplinary Design Optimization (MDO) consists in using optimization methods to solve design problems incorporating a number of disciplines, as well as finding an optimum for the interaction of these disciplines and not for each of them separately. In this case, a modified version of OpenAeroStruct is used, which is a tool based on OpenMDAO. OpenAeroStruct is a global low-fidelity tool that performs aeroestructual optimization, while OpenMDAO is a multidisciplinary design optimization framework developed by NASA. The OpenMDAO framework enable the widespread use of analytic derivatives in MDO applications. This is particularly important because the difficulty of implementing MDO techniques with analytic derivatives created a significant barrier to their adoption by the wider engineering community. One can always compute derivatives using finite differences, but analytic derivative methods are much more efficient and accurate.

2.3 Justification of the potential degree of novelty

The design of HALE drones has already been studied several times. Some global optimizations have been made [2–6]. Even large companies such as Airbus (Figure 1a) or Prismatic (Figure 1b) are manufacturing their first prototypes that are recently starting to fly. However, there is no open-source optimization software for this kind of drones, let alone any software to optimize the environmental footprint of the drones rather than their mass. The work of [1] began to close this gap in a global, low-fidelity but fast, environmental impact optimization. And the aim of this work is to continue their labor.

(a) Airbus-built HALE Zephyr (b) PHASA-35 HALE

Figure 1: Commercial HALE drone prototypes

2.4 Aims and objectives

The main purpose of this project is to refine the modified version of OpenAeroStruct [7–9] presented in [1] in order to obtain better results. The CO_2 footprint optimization of a solar-powered High Altitude Long Endurance (HALE) drone is studied. It is as important to achieve better results as it is to improve the performance of the program and obtain faster optimizations. In consequence, the aim of this work is to achieve a global, fast, low-fidelity but accurate enough CO_2 footprint optimization of a HALE drone.

3 Investigation methods

Where possible, a comparison with Facebook's single-boom HALE, presented in [2], will be made. Therefore, the data from this HALE will be used as a reference to design the different parameters and variables of the optimization and validate the results.

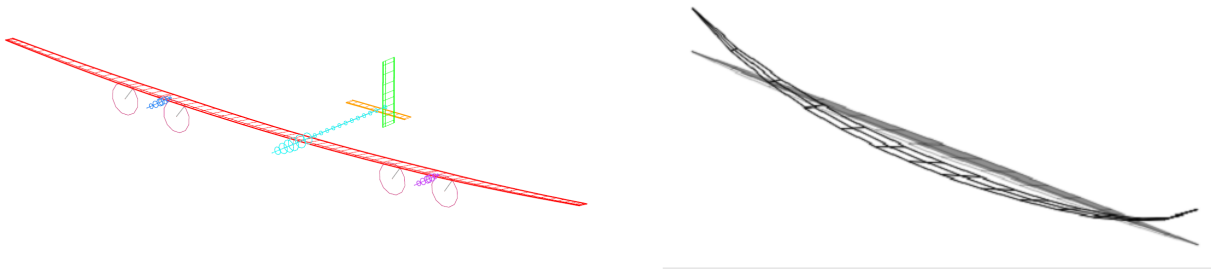

(a) Facebook's single-boom HALE [2] (b) Optimal HALE wing structure [1]

Figure 2: Other HALE drones used for comparison and validation

The work to be done was divided in seven different tasks perfectly differentiated at the beginning of the project. For this reason, this section will include all the tasks that have already been completed.

3.1 Add a constraint to the wing surface

One of the problems that the model presented in [1] has is the *snowball* effect. According to [1]: "A small increase in the drone's weight, leads to an increase of battery and solar panel weight in order to thrust the heavier drone, and an increase of structural weight to lift the heavier drone. These weight increases contribute to a further increase in the drone's weight. This is a *snowball* effect".

By limiting the wing surface, the weight is also limited, preventing the optimization from diverging. Therefore, a constraint of 200 m^2 is added to the code. This number is conservatively chosen based on previous experience and results. For instance, the Facebook's single-boom drone HALE presented in [2] has a wing surface of 72 m^2, while the preliminary results of [1] show a wing surface of 87 m^2. The goal of this threshold is to prevent the optimization from diverging but without affecting the results.

3.2 Fix some design variables

Another way to help convergence consists in fixing some of the design variables which vary less during the optimization process, such as the taper ratio or the root chord. With less design variables, the model should converge much more easily, making the problem more computationally efficient.

However, after some tests, it is checked that the savings in time are not significant since these two design variables converge very quickly and the number of optimizations that finally converge decreases. Thus, in order to be as accurate as possible, and specially for the validation, all the variables have been considered and none of them has been fixed.

3.3 Turn material function into OpenMDAO components

OpenMDAO has a modular implementation. The model is decomposed into *components*. These components are the most efficient way to perform gradient-based optimization. Each component computes the analytic partial derivatives of its outputs with respect to its inputs.

However, the material formulation presented in [1] is performed with a function and not with a component. Thus, this function allows to use the density as the unique material design variable (input) and extract the material data (outputs) such as the Young's modulus, the shear modulus, the yield strength and the CO_2 emissions. Consequently, all the other components that require one or more material properties, have to use the density as an input and call the function to access the other properties. This way, the partial derivatives of the outputs with respect to the density cannot be computed analytically. They are computed numerically through finite difference or complex step methods, which require many calls and evaluations of the function, meaning an increase in computational time.

In consequence, the creation of these four new components (one for each of the properties) allows for faster optimizations by using the material properties (outputs of the new components) as inputs for the other components (structural components) with analytic partial derivatives. In addition, these analytic derivatives have been computed manually and introduced in the code, as well as the connections between the existing components and the new ones. This way, the property that is output of each of the new components must be connected as an input to the other components that have to use its value.

To summarize, now there are four components that have only the density as an input in order to access the material properties database and interpolate. The four properties required (outputs) are the Young's modulus, the shear modulus, the yield strength and the CO_2 emissions per kilogram of material.

The function of [1] and the new components operate in the same manner. As presented in [1]: in order to have only continuous variables (requirement for every gradient-based optimization), the density design variable is made continuous by interpolating each material property in the space among the real materials of the database. To prevent the optimization for choosing an intermediate fictitious material, the interpolation is penalize by the use of a power factor, as shown in Equation 1:

$$\begin{aligned} &X(\rho) = A \cdot \rho^p + B \\ &\text{with} \quad A = \frac{X_{i+1} - X_i}{\rho_{i+1}^p - \rho_i^p} \quad \text{and} \quad B = X_i - A \cdot \rho_i^p \end{aligned} \tag{1}$$

where X is the interpolated material property at density ρ, ρ_i and ρ_{i+1} are the densities of the real materials enclosing the one being interpolated, X_i and X_{i+1} are the respective values of the material property of these real materials, and p is the penalization factor.

Figure 3 comes from [1] and represents the resulting interpolation of the Young's modulus for a penalization factor of 5 ($p = 5$). It is possible to see that, from a real material, a small decrease in density produces a great decrease in Young's modulus, while, a big

increase in density generates a very small increase in Young's modulus. Consequently, fictitious materials are never optimal.

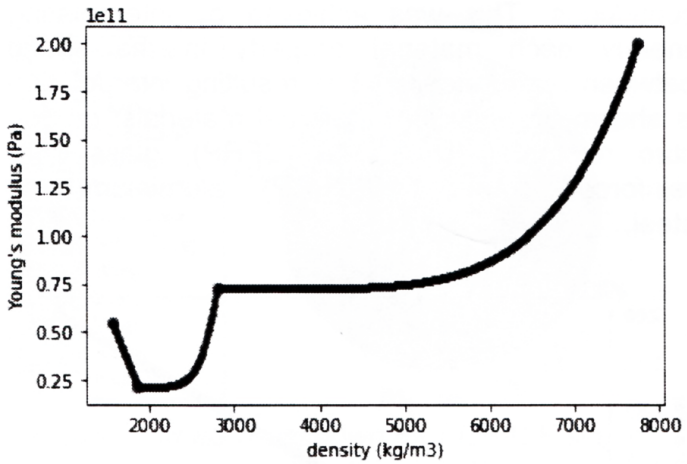

Figure 3: Young's modulus example of penalized interpolation of materials [1]

Furthermore, another goal of this task was to get to know the OpenMDAO methodology and implementation by creating components. It has been very useful for the development of the remaining tasks.

3.4 Add engines as point masses

The principle is to add loads from point masses on to the wing structure. The loads caused by the point masses are transferred to the structural nodes based on the nodes' proximity to the point masses, leading into a more realistic model.

The Facebook's single-boom HALE presented in [2] has two symmetrical engines. Therefore, two point masses have been added, considering the distance from the HALE plane of symmetry as a new design variable to optimize. The aim is to reduce the bending moment on the wing due to lift and, as a result, lower the structural mass of the HALE.

The mass of each engine is considered equal to the one in [1], where the engines are located in the plane of symmetry of the drone. The propulsion mass (M_{prop}) models both the mass of the motors and the propellers. It comes from the power needed for propulsion (that may change at each iteration) and the propulsion density (d_{prop} in kg/W), as shown in Equation 2 (that comes from [1]). The propulsion density is obtained from the validation case, FB HALE [2], dividing the mass of its engines by the power required only for propulsion.

$$M_{prop} = P_{prop} \cdot d_{prop} = P_{prop} \cdot \left(\frac{M_{prop}}{P_{prop}} \right)_{FBHALE} \tag{2}$$

As the HALE has 2 engines:

$$M_{engine} = \frac{M_{prop}}{2} \tag{3}$$

Furthermore, after some optimizations it was noted that the engines, which are very light, were located near the wing tips in most of the cases. For this reason, a new aerostructural point has been added to the problem. This point considers the ground case, where there is no speed and no lift, as a result, the weight of the engines must be supported by the structure. The outcome is a more realistic result of the optimization. Previously, as in [1], only two aerostructural points were considered: one for cruise conditions and other with a vertical uniform gust.

4 Results and analysis

In the same way as in [1], the model is compared with the Facebook's single-boom HALE of [2]. In order for the comparison to be significant, the objective function is changed to do a total mass optimization instead of a CO_2 footprint optimization. For this purpose, the material design variable (material density) is fixed and a material similar to the one of [2] is chosen.

However, the method is based on local optimization. If we aspire to find a global optimum, some type of diversification to overcome local optimality and possible divergences is required. Without this diversification, the method can become localized in a small area of the solution space, eliminating the possibility of finding a global optimum. Therefore, a multistart strategy is used. The main idea of this strategy is to sample the solution space of the problem. Then, an optimization is run from each of these starting points. And finally, all the local optima achieved are compared in order to find the best result, that not necessarily corresponds to the global optimum.

As, there are nine design variables (eight for validation because the material is fixed), it is computationally unviable to choose many starting points for each of them. Especially if we do not want to wait hours or even days for the optimization to finish, since it is a low fidelity model that should achieve results very quickly. Thus, for only some variables, a few multistart values are regularly spread between the higher and the lower limits considered. For the others, only one starting value is taking into account. The starting values for all the design variables, as well as their lower and higher limits are presented in Table 2.

In order for the design variables to be independent of the fidelity of the mesh, they are defined as arrays along the span. There are four control points along the semi-span which influence a b-spline interpolation among the values of the variable at that point. Obviously, this is only needed for the variables that vary along the span. All the design variables are summarized in Table 1.

Table 1: Design variable symbols

Design variable	Symbol
Density	ρ
Twist control points	θ_{cp}
Skin thickness control points	$t_{skin_{cp}}$
Spar thickness control points	$t_{spar_{cp}}$
Thickness over chord ratio control points	$(t/c)_{cp}$
Span	b
Root chord	c_{root}
Taper ratio	λ
Engine spanwise location over semi-span ratio	$y_{engine}/(b/2)$

Table 2: Design variable values for multistart strategy

Design variable	Units	Lower limit	Higher limit	Number of starting values	Starting values
ρ	kg/m^3	Fixed for validation		1	505
θ_{cp}	deg	-30	30	1	[10 20 20 20]
$t_{skin_{cp}}$	m	0.0001	0.1	2	10^{-3}·[1 2 3 4], 10^{-3}·[2 4 6 8]
$t_{spar_{cp}}$	m	0.0001	0.1	2	10^{-4}·[1 1 1 1], 10^{-4}·[3 3 3 3]
$(t/c)_{cp}$	-	0.01	0.4	2	10^{-2}·[3.75 5 5 6.25], 10^{-2}·[9.75 13 13 16.25]
b	m	1	1000	3	50, 75, 100
c_{root}	m	1.4	500	1	1.5
λ	-	0.3	0.99	1	0.3
$y_{engine}/(b/2)$	-	0	1	1	0.3

Every combination of values is used, meaning that a total of $3{\cdot}2{\cdot}2{\cdot}2{\cdot}1^5 = 24$ optimizations are run. Two cases are analysed: with and without engines as point masses. The results of both cases are shown in Table 3. The values of [1] and [2] have been added to Table 3 for comparison. It can be seen that the results without engines are very similar to those of [1], since in essence both optimizations are very similar. Only the new components for material properties, the constraint to the wing surface and the starting values for the design variables are different, the rest of the code is exactly the same. Therefore, the conclusions are identical to those of [1]: the results are in the same order of magnitude as in [2] except for the aspect ratio.

On the contrary, adding the engines as point masses the bending moment on the wing due to lift is reduced and thus, the structural mass also decreases. The results are closer to those of [2]. However, the aspect ratio is lower, but still very high. For this case, with engines as point masses, the other design variables that are not shown in Table 3 are presented in Figure 4 (twist), Figure 5 (skin thickness), Figure 6 (spar thickness), and Figure 7 (thickness over chord ratio). For instance, it is possible to see in these graphs that the skin thickness is much greater than the thickness of the spars. This can be

explained by the buckling model used, that considers the skin between the spars as a flat plate, which is much more restrictive than the model employed in [2].

Table 3: Final design variable values for validation case

Design variable	**Units**	**HALE of [1]**	**FB HALE [2]**	**Results w/o engines**	**Results w/ engines**
Span	m	97.5	-	93.5	70.2
Root chord	m	1.4	-	1.4	1.4
Taper ratio	-	0.32	-	0.33	0.30
Total mass	kg	378	320	435	362
Wing surface	m^2	86.6	71.8	83.4	61.3
Aspect ratio	-	94	29	105	80
C_L^{cruise}	-	1.31	1.33	1.56	1.77
$(C_L^{3/2}/C_D)^{cruise}$	-	44.1	40.1	57.8	72.1
$y_{engine}/(b/2)$	-	0	0.46	0	0.79

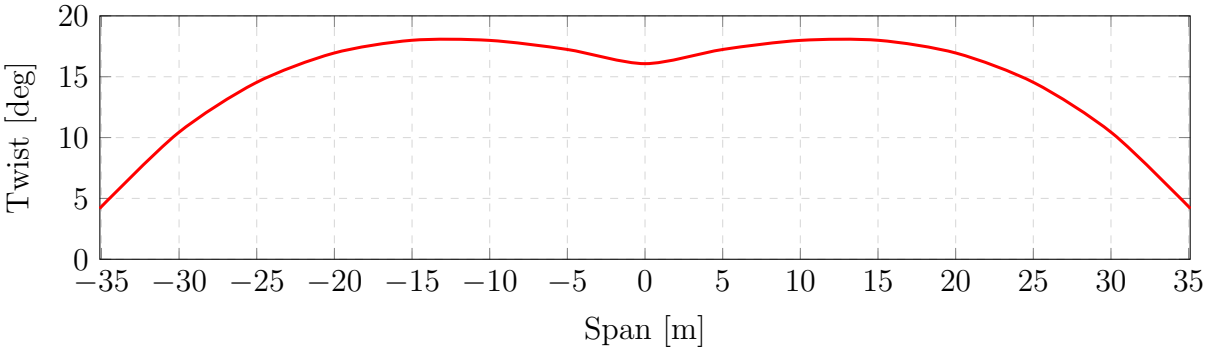

Figure 4: Resulting twist distribution along span for the case with engines as point masses

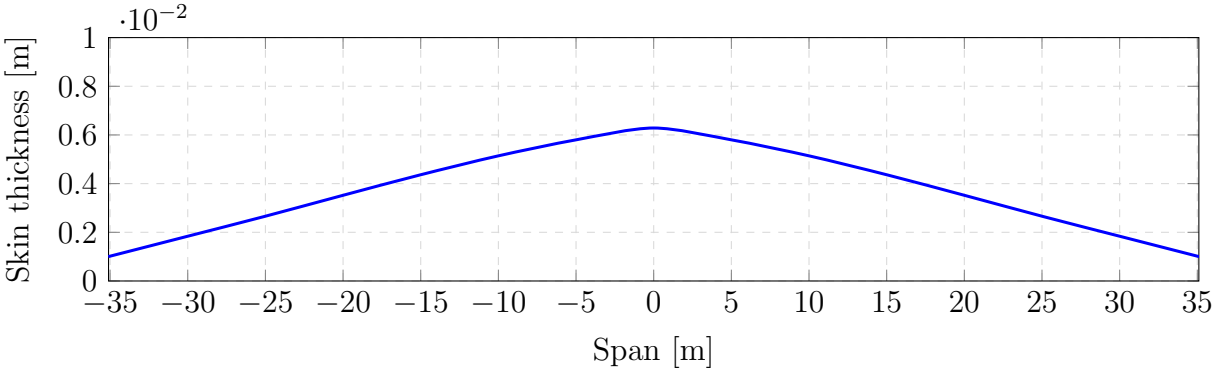

Figure 5: Skin thickness distribution along span for the case with engines as point masses

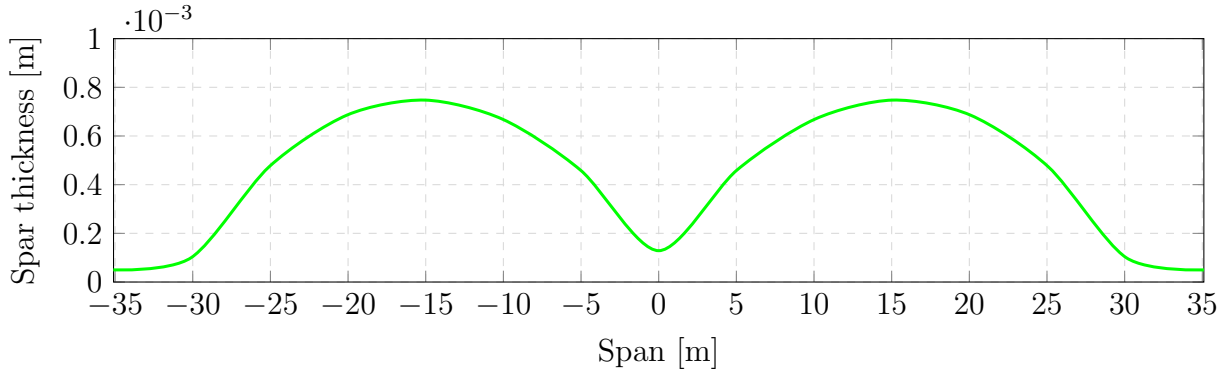

Figure 6: Spar thickness distribution along span for the case with engines as point masses

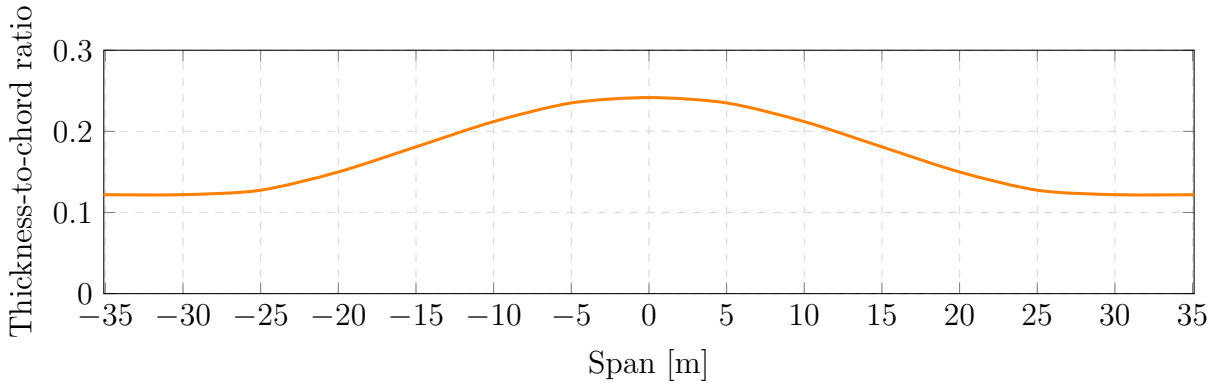

Figure 7: Thickness over chord ratio distribution along span for the case with engines as point masses

Besides, the bending moment distribution for cruise conditions achieved by adding the engines can be seen in Figure 8. Due to the weight of the engines, only 7.8 kg per engine, their optimal position is far from the plane of symmetry of the HALE in order to have a significant effect in the bending moment. All the findings show that the results adding the engines are much better.

For instance, the reduction of the bending moment due to lift at the root of the wing because of the engines is:

$$\Delta M_b^{engine}(y=0) = M_{engine} \cdot g \cdot y_{engine} = 2120 \text{ N} \cdot \text{m} \tag{4}$$

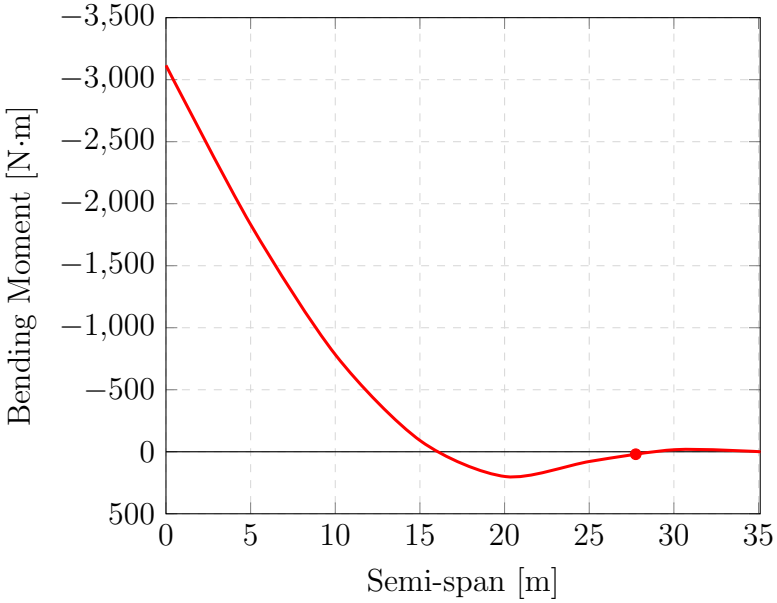

Figure 8: Bending moment distribution along semi-span for cruise conditions and engines as point masses, with $M_{engine} = 7.8$ kg, and $y_{engine} = 27.7$ m

Nevertheless, the most significant changes with respect to [1] are in terms of performance and efficiency of the optimizations. For the same 24 starting values of the design variables, only 7 final convergences were found in 2 hours with the code of [1]. However, as might be expected, only by adding the new components for material properties and the constraint to the wing surface, the number of convergences increases to 12, which represents half of the optimizations performed. The running time of the optimizations also increases to about 3 hours, but this means that the optimizations that do not converge complete more iterations until diverging. So, they are more likely to converge, specially if new tools that help convergence are implemented in the future.

Furthermore, with engines as point masses the results are quite similar. From the same 24 starting values, 11 final convergences are reached in about 4 hours. On the one hand, these point masses help convergence by reducing the bending moment on the wing due to lift. On the other hand, they make the model more complex, since it has one design variable more (eight instead of seven), and, for this reason, it takes more time to converge. This difference in running time could be very small for a single optimization, but, as 24 optimizations are performed, the disparity increases to about one hour. The number of convergences achieved also decreases by one for the same reason.

All the performance results are summarized in Table 4:

Table 4: Performance values for validation case

Performance	**Units**	**HALE of [1]**	**Results w/o engines**	**Results w/ engines**
Optimizations	-	24	24	24
Convergences	-	7	12	11
Time	h	2	3	4

5 Conclusions

Continuing the work of [1], the new components to access material properties allowing gradient-based optimization have been integrated successfully. In addition, two symmetrical engines have been added, considering their spanwise location as a new design variable for the optimization.

The key result is that the performance of the optimization with the new components has improved enormously with respect to [1]. Furthermore, with the engines, the results are much more realistic and closer to those of the Facebook's single-boom HALE [2].

However, as in [1], the main difference with respect to [2] is the aspect ratio. This is due to the differences in the buckling constraint and in the gust model. The buckling constraint taking into account is more restrictive than the one of [2], because we are considering the skin between the spars as a flat plate under axial compression. Moreover, the gust case used corresponds to a shear uniform gust (gust wall), while [2] also takes into account a 1-cosine gust. These two differences under-penalize high aspect-ratios.

6 Perspectives and future work

As commented before, there are three very important remaining task for semester 3 to have a more realistic model and reduce the differences with respect to the validation case of [2].

6.1 Set different materials for different parts of the wing

The main conclusion presented in [1] is: "[...] a material optimal in terms of drone total weight is also optimal in terms of drone total CO_2 emissions [...]". For this reason, it would be very useful to allow the optimization to use different materials for the various parts of the wing (spars and skins) in order to obtain better results.

This approach makes possible to reach a better solution in terms of CO_2 footprint. The findings should also be more accurate. On the other hand, the more design variables the model have, the longer the optimization process takes to complete. So, allowing the optimization to choose two different materials, one for the spars and one for the skins, results in an increase in the design variables by one (a new density for the second material).

6.2 Introduce a more complex buckling model

Presently, a very simple buckling model is used, identical to that in [1]. It takes into account the skins as rectangular flat plates only under axial compression. Considering curved plates under combined axial compression and shear a slightly more complex model is achieved, as the one explained in [10]. It is also said in [10] that: "[...] a long curved plate under shear buckles at a stress in close agreement with the theoretical value derived from linear theory. However, [...] the action of axially compressed long curved plates departs appreciably from the predictions of linear theory. Consequently, a linear analysis of buckling under the combination of these loads would be unconservative". For this reason,

they recommend the use of empirical data.

The idea is to calculate the stresses of axial compression and shear separately (simple loading), and then, impose a parabolic interaction between them. This parabolic interaction is given by Equation 5 proposed in [10]. This expression fits very well with the experimental results as shown in Figure 9.

$$R_S^2 + R_C = 1 \tag{5}$$

where R_S and R_C are the stress ratios for shear and axial compression, respectively. The stress ratios are defined as the ratio of the stress at buckling under combined loading to the buckling stress under simple loading.

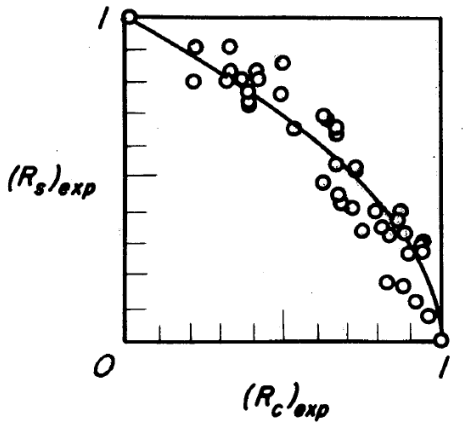

Figure 9: Comparison of test data with parabolic interaction curves for simply supported, curved plates under combined shear and axial compression [10]

It is important to note that, as the Finite Element Method (FEM) approach that OpenAeroStruct implements (explained in [7]) uses spatial beams elements, it is not viable to consider a FEM model for buckling. This is why analytical methods are the best option since they are sufficiently accurate and computationally more efficient, which is necessary to obtain faster optimizations.

6.3 Model a two dimensional discrete gust

As it is mentioned before, the HALE is compared with the Facebook's single-boom HALE, displayed in [2], in order to validate the framework. However, one of the main differences in the results, that also occurred in [1], is the aspect ratio, which is much larger than the one in [2]. As said in [1]: "These differences are mainly due to our not taking into account 1-cosine gusts in our framework [...] which would lead to more stress than a gust wall for a large-span wing".

In an attempt to solve this issue and reach more realistic results, a two dimensional gust will be taken into account. A simplification of the two-dimensional gust profile declared in [11] could be used with a shape given by:

$$w_g(y) = U_{de} \cos\left(\frac{2\pi y}{aL_{span}}\right) \tag{6}$$

where w_g is the gust velocity, U_{de} is the derived equivalent gust velocity, L_{span} is the aircraft span, a is a factor that is used to represent the spanwise distribution of the gust, and y is the spanwise coordinate.

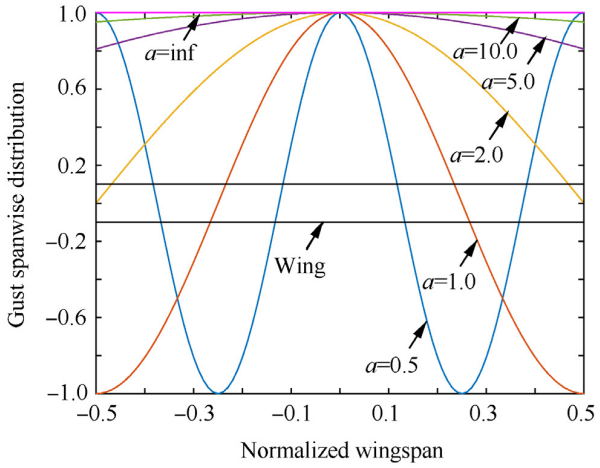

Figure 10: Spanwise distribution of cosine gusts (Normalized wingspan: y/L_{span}, Gust spanwise distribution: $\cos\left(\frac{2\pi y}{aL_{span}}\right)$) [11]

Figure 10 represents the spanwise gust distribution with different values of a. The two-dimensional gust degenerates into the one-dimensional shear gust, currently used in the existing model that comes from [1], when a tends to infinity.

With the intention of increasing the bending moment and penalizing large aspect ratios, another option could be a 1-cosine gust with the highest vertical velocity near the wing tips, depicted in Figure 11 and with a shape given by:

$$w_g(y) = \frac{U_{de}}{2}\left[1 - \cos\left(\frac{2\pi y}{aL_{span}}\right)\right] \tag{7}$$

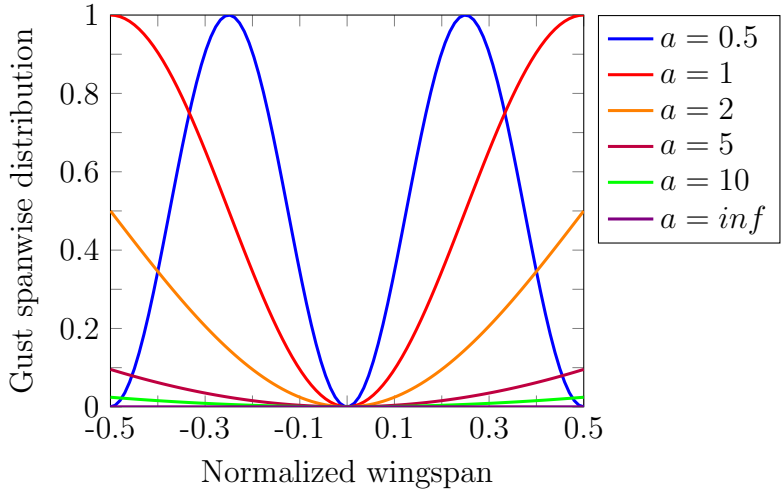

Figure 11: Spanwise distribution of 1-cosine gusts (Normalized wingspan: y/L_{span}, Gust spanwise distribution: $\frac{1}{2}\left[1 - \cos\left(\frac{2\pi y}{aL_{span}}\right)\right]$)

In order to have model conditions as realistic as possible, a gust field distribution orientated normally to the path of the aircraft, as presented in [11], could be added in the future. A two-dimensional gust field has only vertical velocity with time and spanwise amplitude variation. It could be given by Equation 8 shown in [11]. This is the gust field used for sizing the FB HALE [2], as displayed in Figure 12.

$$\begin{cases} w_g(y,t) = U_{SA}\left[1 - cos\left(2\pi\left(\frac{Vt}{L_g}\right)\right)\right]\ \cos\left(\frac{2\pi y}{aL_{span}}\right) & 0 \leq t \leq L_g/V \\ U_{SA} = \frac{U_{de}}{2}(L_{span}/2L_g)^{\frac{1}{3}} \end{cases} \tag{8}$$

where L_g is the gust length, V is the velocity of the aircraft, and t is the flight time.

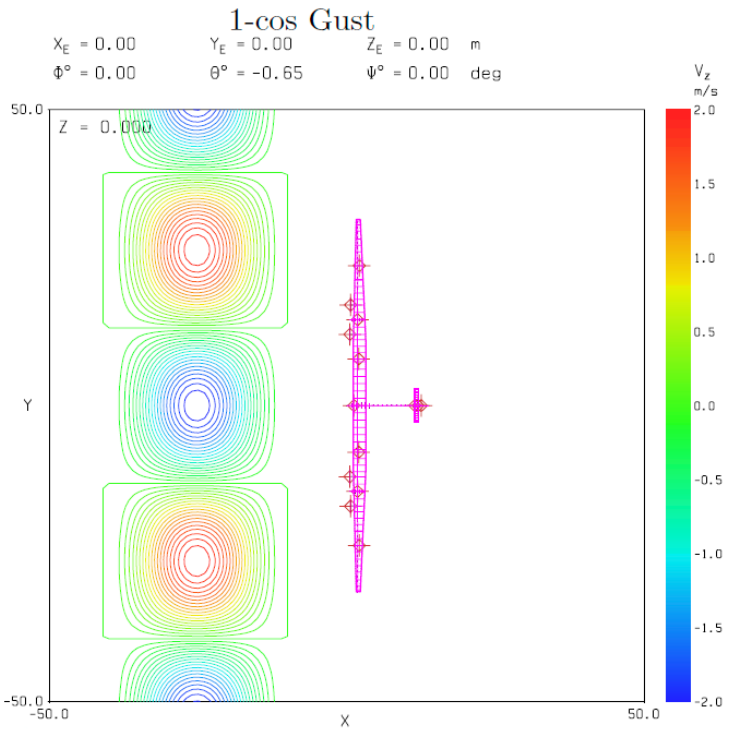

Figure 12: Worst case 1-cos gust for Facebook's single-boom HALE [2]

7 References

[1] E. Duriez and J. Morlier, "HALE multidisciplinary design optimization with a focus on Eco-Material selection," *ISAE Supaero*, 2020.

[2] D. Colas, N. H. Roberts, and V. S. Suryakumar, "HALE multidisciplinary design optimization Part I: Solar-powered single and multiple-boom aircraft," in *2018 Aviation Technology, Integration, and Operations Conference*, p. 3028, 2018.

[3] B. Morrisey and R. McDonald, "Multidisciplinary design optimization of an extreme aspect ratio HALE UAV," in *9th AIAA Aviation Technology, Integration, and Operations Conference (ATIO) and Aircraft Noise and Emissions Reduction Symposium (ANERS)*, p. 6949, 2009.

[4] O. Montagnier and L. Bovet, "Optimization of a solar-powered high altitude long endurance UAV," in *Proc. 27th International Congress of The Aeronautical Sciences*, 2010.

[5] A. Noth, *Design of solar powered airplanes for continous flight*. PhD thesis, ETH Zurich, 2008.

[6] E. M. Botero, A. Wendorff, T. MacDonald, A. Variyar, J. M. Vegh, T. W. Lukaczyk, J. J. Alonso, T. H. Orra, and C. Ilario da Silva, "SUAVE: An open-source environment for conceptual vehicle design and optimization," in *54th AIAA Aerospace Sciences Meeting*, p. 1275, 2016.

[7] J. P. Jasa, J. T. Hwang, and J. R. Martins, "Open-source coupled aerostructural optimization using Python," *Structural and Multidisciplinary Optimization*, vol. 57, no. 4, pp. 1815–1827, 2018.

[8] S. S. Chauhan and J. R. Martins, "Low-fidelity aerostructural optimization of aircraft wings with a simplified wingbox model using OpenAeroStruct," in *International Conference on Engineering Optimization*, pp. 418–431, Springer, 2018.

[9] J. P. Jasa, S. S. Chauhan, J. S. Gray, and J. Martins, "How certain physical considerations impact aerostructural wing optimization," in *AIAA Aviation 2019 Forum*, p. 3242, 2019.

[10] G. Gerard and H. Becker, "Handbook of Structural Stability. Part 3. Buckling of Curved Plates and Shells.," tech. rep., NATIONAL AERONAUTICS AND SPACE ADMINISTRATION WASHINGTON DC, 1957.

[11] Y. Yang, Y. Chao, and W. Zhigang, "Aeroelastic dynamic response of elastic aircraft with consideration of two-dimensional discrete gust excitation," *Chinese Journal of Aeronautics*, 2019.